DALTON
FULL PAPER

New tetranuclear metal carboxylate clusters with the $[M_4(\mu_3\text{-}O)_2]^{8+}$ (M = Mn^{III} or Fe^{III}) cores: crystal structures and properties of $[Mn_4O_2Cl_2(O_2CC_6H_3F_2\text{-}3,5)_6(py)_4]$, $[Fe_4O_2Cl_2(O_2CMe)_6(bpy)_2]$ and $[NBu^n_4][Fe_4O_2(O_2CMe)_7(pic)_2]$ †

Michael W. Wemple,[a] DeAnna K. Coggin,[a] John B. Vincent,[a] James K. McCusker,[b] William E. Streib,[a] John C. Huffman,[a] David N. Hendrickson *,[b] and George Christou *,[a]

[a] *Department of Chemistry and Molecular Structure Center, Indiana University, Bloomington, Indiana 47405-4001, USA*
[b] *Department of Chemistry, 0358, University of California at San Diego, La Jolla, California 92093-0358, USA*

A variety of synthetic procedures have been employed that allow access to three new tetranuclear $[M_4(\mu_3\text{-}O)_2]^{8+}$ (M = Mn^{III} or Fe^{III}) complexes. The complex $[Fe_4O_2Cl_2(O_2CMe)_6(bpy)_2]$ displays an unusual structural asymmetry in its core that can be described as a hybrid of the bent (butterfly) and planar dispositions of four M atoms seen previously in such compounds. Magnetochemical and ^{57}Fe Mössbauer studies on this compound showed that its structural asymmetry has little influence on these properties compared with the more symmetric types. The complex $[NBu^n_4][Fe_4O_2(O_2CMe)_7(pic)_2]$ has been prepared by an unusual chelate substitution in $[NBu^n_4][Fe_4O_2(O_2CMe)_7(bpy)_2]$ that does not disrupt the core or the bridging carboxylate groups.

Tetranuclear, oxide-bridged carboxylate clusters of Fe^{III} or Mn^{III} with a butterfly disposition of four metal ions have been under study for several years and have yielded a wealth of interesting structural, spectroscopic and physical data. The first example for Fe^{III} was $[Fe_4O_2(O_2CCF_3)_8(H_2O)_6]$ reported in 1984[1] and this was followed soon after by a number of other examples such as $[NEt_4][Fe_4O_2(O_2CR)_7\{H_2B(pz)_2\}_2]$ [$H_2B(pz)_2^-$ = dihydrobis(pyrazol-1-yl)borate; R = Me or Ph],[2] $[Fe_4O_2(O_2CMe)_7(bpy)_2]ClO_4$ **1** (bpy = 2,2′-bipyridine),[3] $[Fe_4O_2(O_2CMe)_3L_2(sao)_2]PF_6$ (L = 1,4,7-trimethyl-1,4,7-triazacyclononane; sao^{2-} = dianion of salicylaldoxime)[4] and $[Fe_4O_2Cl_2(O_2CMe)_6(NC_5H_4Me\text{-}3)_4]$.[5] The compound $[Fe_4O_2(O_2CPh)_4(bicoh)_2(bico)_2]Cl_2$ [bicoh = bis(*N*-methylimidazol-2-yl)methanol] also has a $[Fe_4O_2]^{8+}$ core but with a planar Fe_4 unit.[6]

In manganese(III) chemistry the first example was $[Mn_4O_2(O_2CMe)_7(bpy)_2]ClO_4$ **2** reported in 1987,[7] and there have been a number of additional examples since, some planar, including $[NR_4][Mn_4O_2(O_2CMe)_7(L{-}L)_2]$ [L–L = pyridine-2-carboxylate (picolinate),[8] anion of 2-hydroxymethylpyridine[9] or 8-hydroxyquinolinate],[9] $[NBu^n_4][Mn_4O_2(O_2CPh)_9(H_2O)]$,[10] $[Mn_4O_2L_2][PF_6]_2$,[11] $[Mn_4O_2(O_2CMe)_2L'_2]$[12] and $[Mn_4O_2L''_2][CF_3SO_2]_2$,[13] where L, L′ and L″ are polydentate ligands. Mixed-valent varieties ($2Mn^{II}$, $2Mn^{III}$) are also known in $[Mn_4O_2(O_2CCPh_3)_6(Et_2O)_2]$[14] and $[Mn_4O_2(O_2CMe)_6(bpy)_2]$,[7] which have a planar Mn_4 unit.

More recently, analogous $[Cr_4O_2]^{8+}$ and $[V_4O_2]^{8+}$ complexes have been prepared, as in $[Cr_4O_2(O_2CMe)_7(bpy)_2]^+$[15] and $[V_4O_2(O_2CEt)_7(bpy)_2]^+$[16] salts and similar species. We herein report the preparation of three new $[M_4O_2]^{8+}$ species, two of which contain terminal Cl^- ions that yield interesting structures and which should make these complexes useful as stepping stones to new complexes in the future. We also show that exchange of the bpy in **1** is possible with picolinate (pic^-) to yield the new iron(III) butterfly complex $[NBu^n_4][Fe_4O_2(O_2CMe)_7(pic)_2]$.

† *Non-SI unit employed*: $\mu_B \approx 9.27 \times 10^{-24}$ J T^{-1}.

Experimental

General

All manipulations were performed under aerobic conditions, except where specified otherwise, and all chemicals used as received. The compounds $[Fe_4O_2(O_2CMe)_7(bpy)_2]ClO_4$ **1**,[3] $[Mn_4O_3Cl_4(O_2CMe)_3(py)_3]$[17] and $[Fe_2OCl_2(O_2CMe)_2(bpy)_2]$[18] were available from previous work; $C_6H_3F_2CO_2H$ is 3,5-difluorobenzoic acid; Hpic is picolinic acid.

Preparations

$Mn(O_2CC_6H_3F_2)_2{\cdot}2H_2O$. Manganese(II) carbonate (1.0 g, 8.7 mmol) and 3,5-difluorobenzoic acid (1.0 g, 6.3 mmol) were refluxed in water (50 cm^3) for 2 d. Unchanged $MnCO_3$ was removed by filtration and washed with water. The wash was combined with the filtrate, which was then taken to dryness. The resulting pale pink solid was washed with hexanes to remove unchanged acid. The yield was 0.93 g, 79% based on the available carboxylic acid (Found: C, 41.31; H, 2.50. $C_{14}H_{10}F_4MnO_6$ requires C, 41.50; H, 2.49%).

$[NBu^n_4][Mn_4O_2(O_2CC_6H_3F_2)_9(H_2O)]$. This synthesis closely parallels that of $[NBu^n_4][Mn_4O_2(O_2CPh)_9(H_2O)]$.[10] The compounds $Mn(O_2CC_6H_3F_2)_2{\cdot}2H_2O$ (0.82 g, 2.0 mmol) and 3,5-difluorobenzoic acid (2.43 g, 15.4 mmol) were dissolved in a mixture of MeCN (10 cm^3) and EtOH (5 cm^3). Solid $NBu^n_4MnO_4$ (0.29 g, 0.80 mmol) was slowly added with stirring, and the solvent then evaporated under reduced pressure. The residue was dissolved in CH_2Cl_2 (30 cm^3), filtered, and the filtrate layered with pentane (30 cm^3) slowly to give a red-brown oil over the course of 2 d. The oil was repeatedly washed with pentane until a powder was obtained and the latter collected by filtration and dried *in vacuo*. The yield was 77% based on available Mn (Found: C, 49.52; H, 3.40; N, 0.72. $C_{79}H_{65}F_{18}Mn_4NO_{21}$ requires C, 49.26; H, 3.40; N, 0.73%). This product is very hygroscopic and was therefore stored under N_2.

$[Mn_4O_2Cl_2(O_2CC_6H_3F_2)_6(py)_4]$ 3. *Procedure* 1. A slurry of $[Mn_4O_3Cl_4(O_2CMe)_3(py)_3]$ (0.90 g, 1.0 mmol) and 3,5-difluorobenzoic acid (0.62 g, 4.0 mmol) in toluene (50 cm^3) was stirred for at least 1 h at ambient temperature to give a brown precipitate and a dark brown solution. The solvent was removed under vacuum, the resulting residue redissolved in toluene (40 cm^3), and the solvent then removed again under vacuum. This step was repeated three times. The solid was then extracted with diethyl ether and the remaining solid washed with pentane. This solid has been characterised previously[19] as $[Mn_4O_3Cl_4(O_2CC_6H_3F_2)_3(py)_3]$; the yield was 0.82 g, 71%. The red-brown ether solution was layered with an equal volume of pentane slowly to give X-ray-quality crystals of **3**·2Et_2O, which were collected by filtration and washed with a little pentane. Yield 11%. Dried solid loses the ether of crystallisation (Found: C, 46.97; H, 2.59; Cl, 4.65; N, 3.50. $C_{31}H_{19}ClF_6Mn_2N_2O_7$ requires C, 47.08; H, 2.42; Cl, 4.48; N, 3.54). For crystallographic characterisation the sample was stored in the mother-liquor to prevent solvent loss.

Procedure 2. Under a nitrogen atmosphere, $[NBu^n_4][Mn_4O_2(O_2CC_6H_3F_2)_9(H_2O)]$ (0.24 g, 0.13 mmol) was dissolved in Et_2O (25 cm^3, distilled over sodium–benzophenone). Pyridine (41 μL, 0.51 mmol) was added to the solution, followed by Me_3SiCl (35 μL, 0.28 mmol). After 10 min of stirring at ambient temperature a brown oil was removed by decanting, and the solution was layered with hexanes (25 cm^3, distilled from sodium–benzophenone) to give complex **3**. Yield 20% (Found: C, 47.1; H, 2.7; Cl, 4.4; N, 3.3%). The product gave an IR spectrum identical to that for material from Procedure 1.

$[Fe_4O_2Cl_2(O_2CMe)_6(bpy)_2]$ 4. *Procedure* 1. A stirred yellow solution of $FeCl_2$·$4H_2O$ (2.50 g, 12.6 mmol) in EtOH (125 cm^3) was treated with NaO_2CMe (1.60 g, 19.5 mmol). After 5 min bpy (0.98 g, 6.3 mmol) was added to the brown reaction mixture, and the resultant red mixture was stirred overnight, filtered, and the filtrate evaporated to an oil under vacuum. The oil was redissolved in CH_2Cl_2 (40 cm^3) and filtered to remove a red powder. Layering of the CH_2Cl_2 filtrate with an equal volume of hexanes slowly gave red-brown crystals and an oil after 1 week. The crystals were collected by filtration and recrystallized again from CH_2Cl_2–hexanes to give dark red crystals which were collected by filtration, washed with hexanes, and dried *in vacuo*. Yield, 35%. The dried solid analysed as **4**·0.25CH_2Cl_2·H_2O (Found: C, 37.1; H, 3.45; Cl, 8.3; Fe, 22.0; N, 5.1. $C_{32.25}H_{36.5}Cl_{2.5}Fe_4N_4O_{15}$ requires C, 37.5; H, 3.6; Cl, 8.6; Fe, 21.6; N, 5.4%). The crystallography sample was kept in contact with mother-liquor to avoid solvent loss, and it was subsequently identified as **4**·5CH_2Cl_2.

Procedure 2. A mixture of $[Fe_2OCl_2(O_2CMe)_2(bpy)_2]$·0.5MeCN·$2H_2O$ (0.27 g, 0.39 mmol) in CH_2Cl_2 (20 cm^3) was treated with NaO_2CMe (0.070 g, 0.85 mmol) and $NBu^n_4ClO_4$ (0.090 g, 0.26 mmol) and stirred for 15 min. The green-brown mixture was filtered to remove a white solid and the filtrate was layered with an equal volume of hexanes to give red-brown crystals after 5 d. Yield, 75%. Dried solid analysed as **4**·H_2O (Found: C, 38.13; H, 3.50; N, 5.85. $C_{32}H_{36}Cl_2Fe_4N_4O_{15}$ requires C, 38.01; H, 3.59; N, 5.54%). The IR spectrum was identical to that for material from Procedure 1.

$[NBu^n_4][Fe_4O_2(O_2CMe)_7(pic)_2]$ 5. *Procedure* 1. A green-brown solution of compound **1** (0.54 g, 0.50 mmol) and NBu^n_4Cl (0.428 g, 1.54 mmol) in MeCN (50 cm^3) was treated with a solution of Na(pic) (0.150 g, 1.03 mmol) in MeOH (5 cm^3) to give a colour change to orange-brown and a fine precipitate of NaCl. After 3 h the solvent was removed *in vacuo*, the residue dissolved in MeCN (20 cm^3), filtered to remove a fine yellow powder, and the filtrate layered with 3 volume equivalents of Et_2O–hexanes (2:1). After several days dark orange-red crystals were collected by filtration, washed with hexanes, and dried *in vacuo*. The yield was 54%. Dried solid analysed as **5**·0.5Et_2O (Found: C, 44.3; H, 5.8; Fe, 18.7; N, 3.3. $C_{44}H_{70}Fe_4N_3O_{20.5}$ requires C, 44.3; H, 5.9; Fe, 18.7; N, 3.5%). A sample suitable for crystallography was obtained from a slow crystallisation from MeCN–Et_2O–hexanes and was crystallographically determined to be solvate-free.

Procedure 2. A stirred orange solution of $FeCl_3$·$6H_2O$ (10.8 g, 40.0 mmol) in MeCN (400 cm^3) was treated with NaO_2CMe (9.02 g, 110 mmol), NBu^n_4Cl (4.17 g, 15.0 mmol) and glacial $MeCO_2H$ (8 cm^3). The slurry was stirred for 3 h, and then a solution of Na(pic) (2.90 g, 20.0 mmol) in water (5 cm^3) was added and the slurry stirred overnight. The mixture was filtered, the orange-brown filtrate concentrated to ≈100 cm^3 by rotary evaporation, and Et_2O (200 cm^3) added. The solution was refiltered to remove a small amount of powder that had appeared, and the filtrate stored at 4 °C overnight. The orange-brown microcrystals were collected by filtration, dissolved in CH_2Cl_2 (50 cm^3) and layered with an equal volume of hexanes. After several days orange-brown crystals were collected by filtration. The filtrate was layered with additional hexanes (50 cm^3) to give an additional crop of product. The combined solids were recrystallised again from CH_2Cl_2–hexanes. The final yield of complex **5** was ≈70%. The IR spectrum was identical with that for material prepared by Procedure 1.

$[NBu^n_4][Fe_4O_2(O_2CPh)_7(pic)_2]$ 6. A stirred brown solution of complex **5** (0.29 g, 0.25 mmol) in CH_2Cl_2 (25 cm^3) was treated with solid benzoic acid (0.43 g, 3.5 mmol). After 1 h hexanes (75 cm^3) were slowly added to precipitate a brown powder, which was collected by filtration, washed copiously with Et_2O and dried *in vacuo*. The yield was 65–70%. The powder can be recrystallised from a CH_2Cl_2–Et_2O–hexanes (2:1:3) layering. The solid analysed as **6**·3H_2O (Found: C, 56.3; H, 4.9; N, 2.5. $C_{77}H_{85}Fe_4N_3O_{23}$ requires C, 56.3; H, 5.2; N, 2.6%).

X-Ray crystallography

Data were collected at low temperature on a Picker four-circle diffractometer; details of the diffractometry, low-temperature facilities, and computational procedures employed by the Indiana University Molecular Structure Center are available elsewhere.[20a] Suitable crystals were located, affixed to glass fibers using silicone grease, and transferred to the goniostat where they were cooled for characterization and data collection. Data were corrected for Lorentz-polarization effects, and equivalent data averaged. The structures were solved by direct methods (MULTAN 78)[21] and Fourier-difference techniques, and refined[20b] on F by full-matrix least-squares cycles (Table 1).

For complex **3**·2Et_2O a systematic search located a set of diffraction maxima, indicating one of the two triclinic space groups. Subsequent successful solution and refinement of the structure confirmed the centrosymmetric choice, $P\bar{1}$. Following data collection ($+h$, $\pm k$, $\pm l$; $6 \leqslant 2\theta \leqslant 45°$) and averaging of equivalent reflections ($R_{av} = 0.075$), the structure was readily solved without problem, and all non-hydrogen atoms were readily located, including those for two lattice Et_2O molecules. Hydrogen atoms were placed in fixed, idealized positions for the final refinement cycles. A final Fourier-difference map was essentially featureless, the largest peak being 0.35 e $Å^{-3}$.

For complex **4**·5CH_2Cl_2 lattice CH_2Cl_2 is lost extremely rapidly and particular care had to be taken to keep crystals in contact with mother-liquor. A systematic search revealed Laue symmetry and systematic absences consistent with monoclinic space group $P2_1/a$, which was confirmed by the successful structure determination. Four standards measured every 300 data showed an unusually large drift. This was almost certainly due to loss of lattice CH_2Cl_2; the overall loss of intensity for the standards varied from 34 to 56% and averaged a little less than 50%. An anisotropic drift correction was made in an attempt to improve the data. No correction was made for absorption. After data collection ($+h$, $+k$, $\pm l$; $6 \leqslant 2\theta \leqslant 45°$) and averaging

of equivalent reflections (R_{av} = 0.145) the structure was solved and the non-hydrogen atoms of the Fe_4 molecule were easily located. Subsequent Fourier-difference maps revealed five CH_2Cl_2 molecules in the asymmetric unit. Some of these molecules are incomplete, some are disordered, and all have partial occupancy. None of the hydrogen atoms could be located in the Fourier-difference maps and none was included in the refinement. In the final cycles of refinement the atoms of the Fe_4 molecule were varied with anisotropic thermal parameters and the atoms of the CH_2Cl_2 groups were varied with isotropic thermal parameters. The final Fourier-difference map had a few residual peaks of 1.8 e Å^{-3} or less in the vicinity of the CH_2Cl_2 molecules. All other residual peaks were less than 1 e Å^{-3}.

For complex **5** a systematic search located a set of diffraction maxima indicating a triclinic space group. Subsequent solution and refinement of the structure confirmed centrosymmetric $P\bar{1}$ as the correct space group. After data collection ($+h$, $\pm k$, $\pm l$; $6 \leqslant 2\theta \leqslant 45°$), and averaging of equivalent reflections (R_{av} = 0.046) all non-hydrogen atoms were readily located and were refined with anisotropic thermal parameters. All hydrogen atoms were clearly visible in a Fourier-difference map phased on the non-hydrogen atom parameters, and all hydrogen atoms were placed in fixed, idealized positions for the final refinement cycles. A final Fourier-difference map was featureless, with the largest peak being 0.45 e Å^{-3}. No absorption correction was performed.

CCDC reference number 186/825.

Physical measurements

The IR spectra were recorded as Nujol mulls on a Nicolet 510P FTIR spectrophotometer. Variable-temperature magnetic measurements were made on a model VTS-900 SQUID susceptometer. Diamagnetic corrections were estimated from Pascal's constants. Variable-temperature Mössbauer spectra were obtained by using a constant-acceleration vertical drive spectrometer described previously.[22] The sample temperature was controlled by using a Lake Shore Cryogenics model DRC80C temperature controller in conjunction with a silicon diode mounted on the copper sample holder. The absolute accuracy is estimated at ±3 K. The spectra were fit to Lorentzian line shapes using a modified version of a previously reported computer program.[23] Isomer shift values are reported relative to iron foil at 300 K and have not been corrected for the temperature-dependent second-order Doppler shift.

Results and Discussion

Syntheses

The $4Mn^{III}$ complex $[Mn_4O_2(O_2CMe)_7(bpy)_2]ClO_4$ **2** containing a $[Mn_4(\mu_3\text{-}O)_2]^{8+}$ butterfly core was prepared several years ago[7] and presaged a family of related species, none of which contains Cl^- ligands. Interestingly, however, the reaction in CH_2Cl_2 of NEt_4Cl with $[Mn_4O_2(O_2CMe)_6(py)_2(dbm)_2]$ (Hdbm = dibenzoylmethane) gives a heptanuclear Cl-free product $[NEt_4][Mn_7O_4(O_2CMe)_{10}(dbm)_4]$,[24] and this reaction is thought to proceed *via* a Cl-bound intermediate, although no such species could be isolated. Thus, it was of interest when the Cl-containing complex $[Mn_4O_2Cl_2(O_2CC_6H_3F_2)_6(py)_4]$ **3** was first encountered by chance as a minor product in the ligand-exchange reaction between the $3Mn^{III},Mn^{IV}$ complex $[Mn_4O_3Cl_4(O_2CMe)_3(py)_3]$ and 3,5-difluorobenzoic acid. This procedure represents, in general, a convenient method of introducing a number of different carboxylate groups onto the $[Mn_4O_3Cl]^{6+}$ distorted-cubane core,[19] but with $HO_2CC_6H_3F_2$ (and the corresponding 3,5-dichlorobenzoic acid) it was noticed that the filtrates obtained after collection of product crystals were still intensely coloured. Subsequent work-up of the filtrate led to attainment of ether-soluble complex **3** in low (11%) yield. The precise means of its formation from the $[Mn_4O_3Cl]^{6+}$ precursor is undoubtedly complex, but it may be initiated by protonation of core oxide ions, facilitated by the low pK_a values of these acids, triggering reduction and a decrease in the oxide content. Attempts to increase the yield of **3** by addition of reducing agents had no effect.

A synthesis of complex **3** that gives slightly better yields (≈20%) was subsequently developed using $[NBu^n_4][Mn_4O_2(O_2CC_6H_3F_2)_9(H_2O)]$, which already contains the desired $[Mn_4O_2]^{8+}$ core. Addition of 4 equivalents of py and 2 equivalents of Me_3SiCl (the latter to abstract carboxylate groups and provide the required Cl^- ions) to a Et_2O solution of $[NBu^n_4][Mn_4O_2(O_2CC_6H_3F_2)_9(H_2O)]$ gives a solution from which **3** can be isolated by addition of hexanes.

Preparation of the analogous Br^- complex was attempted by employing Me_3SiBr in place of Me_3SiCl; however, this was unsuccessful. One product isolated from this reaction was the $4Mn^{II},2Mn^{III}$ complex $[Mn_6O_2(O_2CC_6H_3F_2)_{10}(py)_4]$, the $PhCO_2^-$ analogue of which is known.[25] This lower-oxidation-state product suggests that Br^- may be too good a reducing agent in this reaction system.

The related $4Fe^{III}$ dichloro complex $[Fe_4O_2Cl_2(O_2CMe)_6(bpy)_2]$ **4** is also attainable *via* two procedures. Earlier work had shown that $[Fe_4O_2(O_2CMe)_7(bpy)_2]ClO_4$ **1** can be converted into $[Fe_2OCl_2(O_2CMe)_2(bpy)_2]$[18] by addition of bpy and Cl^-. It seemed reasonable that the reverse transformation might also be possible by removal of Cl^-; this had, in fact, already been demonstrated for Mn in the conversion of $[Mn_2OCl_2(O_2CMe)_2(bpy)_2]$ into $[Mn_4O_2(O_2CMe)_7(bpy)_2]ClO_4$ **2** by addition of NaO_2CMe–$MeCO_2H$ and $NaClO_4$.[26] However, it was found that treatment of $[Fe_2OCl_2(O_2CMe)_2(bpy)_2]$ with NaO_2CMe and ClO_4^- did not give **2** but instead **4** in high yield (75%). The transformation is summarised in equation (1). The same

$$2\,[Fe_2OCl_2(O_2CMe)_2(bpy)_2] + 2\,NaO_2CMe \longrightarrow [Fe_4O_2Cl_2(O_2CMe)_6(bpy)_2] + 2\,NaCl + 2\,bpy \quad (1)$$

complex is also available by aerial oxidation of a $FeCl_2$–NaO_2CMe–bpy reaction mixture in EtOH; the yield is inferior for the latter method, but it has the advantage of not requiring the prior isolation of $[Fe_2OCl_2(O_2CMe)_2(bpy)_2]$.

The reaction between complex **1** and picolinate unexpectedly gave chelate exchange leading to formation of $[NBu^n_4][Fe_4O_2(O_2CMe)_7(pic)_2]$ **5** in good yield after recrystallization (54%); we had anticipated that core disruption might have occurred to give a mixed-chelate Fe_2 product. With **5** identified, a direct procedure from the appropriate components provided a more convenient and higher yield (70%) synthesis of this complex. Carboxylate substitution can be effected on treatment of **5** with benzoic acid to give $[NBu^n_4][Fe_4O_2(O_2CPh)_7(pic)_2]$ **6**, as summarised in equation (2). Similar carboxylate-exchange reactions have been previously demonstrated for **1** and **2**.[3,7]

$$[Fe_4O_2(O_2CMe)_7(pic)_2]^- + 7\,PhCO_2H \longrightarrow [Fe_4O_2(O_2CPh)_7(pic)_2]^- + 7\,MeCO_2H \quad (2)$$

Crystal structures

The ORTEP representations of complexes **3**, **4** and the anion of **5** are shown in Figs. 1–3, respectively. Selected interatomic distances are listed in Tables 2–4.

Compound **3**·2Et_2O crystallises in triclinic space group $P\bar{1}$. There is a $[Mn_4(\mu\text{-}O)_2]^{8+}$ butterfly core with each body–wingtip Mn_2 pair bridged by a RCO_2^- group in its common *syn*,*syn* binding mode. Six-co-ordinate, near-octahedral geometry at each Mn^{III} is completed by a terminal py group at the body positions [Mn(2) and Mn(3)] and terminal Cl^- and py groups at the wingtip position [Mn(1) and Mn(4)]. The μ_3-O^{2-} ions O(5) and O(6) on each Mn_3 wing of the butterfly are 0.326 and 0.389 Å, respectively, above their Mn_3 least-squares planes. The dihedral angle between these two Mn_3 planes is 142.15°. Each Mn^{III} shows clear

Table 1 Crystallographic data for complexes **3**·2Et_2O, **4**·5CH_2Cl_2 and **5**

	3	**4**	**5**
Formula [a]	$C_{70}H_{58}F_{12}Mn_4N_4O_{16}$	$C_{37}H_{44}Cl_{12}Fe_4N_4O_{14}$	$C_{42}H_{65}Fe_4N_3O_{20}$
M	1729.88	1417.60	1155.40
Space group	$P\bar{1}$	$P2_1/a$	$P\bar{1}$
a/Å	15.893(5)	16.764(22)	12.468(3)
b/Å	17.285(5)	17.830(24)	18.167(4)
c/Å	13.856(4)	17.752(23)	12.225(3)
α/°	97.25(1)		106.89(1)
β/°	104.26(1)	92.24(6)	101.51(1)
γ/°	93.53(1)		75.53(1)
U/Å^3	3642	5302	2541
Z	2	4	2
T/°C	−171	−149	−155
λ [b]/Å	0.710 69	0.710 69	0.710 69
ρ_{calc}/g cm^{-3}	1.577	1.776	1.510
μ/cm^{-1}	8.203	17.462	6.265
Unique data	9473	6995	6638
Observed data	6646 [c]	2999 [d]	5038 [c]
$R(R')$ [e]	0.0622 (0.0561)	0.0936 (0.0969)	0.0617 (0.0598)

[a] Including solvate molecules. [b] Mo-Kα radiation, graphite monochromator. [c] $F > 2.33\sigma(F)$. [d] $F > 3\sigma(F)$. [e] $R = \Sigma ||F_o| - |F_c||/\Sigma|F_o|$, $R' = [\Sigma w(|F_o| - |F_c|)^2/\Sigma w|F_o|^2]^{\frac{1}{2}}$ where $w = 1/\sigma^2(|F_o|)$.

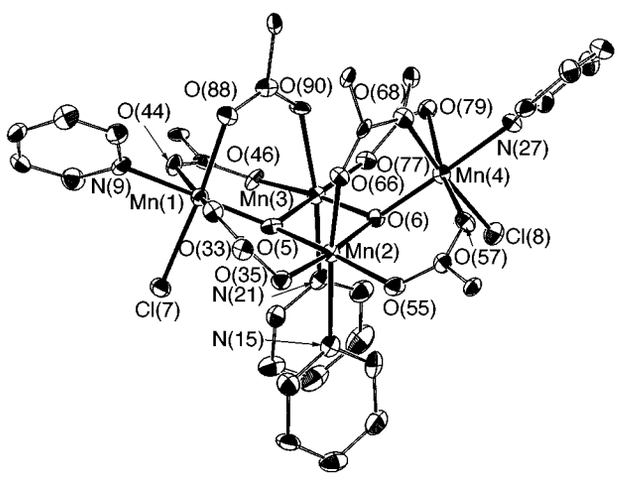

Fig. 1 An ORTEP representation of complex **3**. Thermal ellipsoids are at the 50% probability level

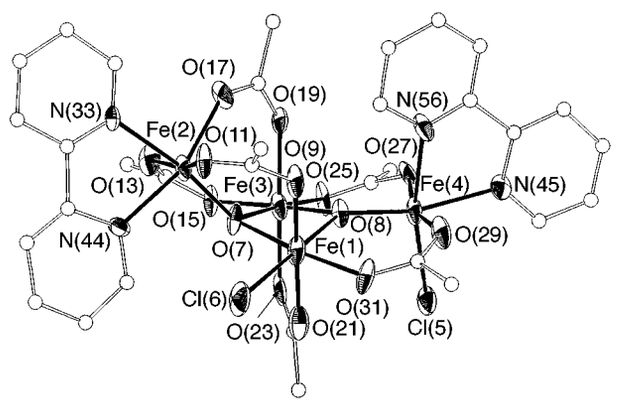

Fig. 2 An ORTEP representation of complex **4**. Thermal ellipsoids are at the 50% probability level except for carbon atoms, which are represented as spheres of arbitrary size

evidence for a Jahn–Teller distortion, as expected for a high-spin d^4 ion in octahedral geometry, taking the form of an axial elongation along the O(33)–Mn(1)–O(44), N(15)–Mn(2)–O(66), N(21)–Mn(3)–O(90) and O(57)– Mn(4)–O(79) axes. Thus, these axial Mn–O,N bonds are 0.1 to 0.2 Å or more longer than equatorial bonds, with the exception of equatorial Mn–Cl bonds which are ≈2.3 Å long; the latter, however, is a normal Mn^{III}–Cl bond length, Jahn–Teller elongated Mn^{III}–Cl bonds being 2.5 to 2.6 Å long.[17,19,26] The complete molecule has virtual C_2 symmetry. Complex **3** represents only the second $[Mn_4O_2]^{8+}$ butterfly to have no chelating peripheral ligands, the other example being $[NBu^n_4][Mn_4O_2(O_2CPh)_9(H_2O)]$ (although even in the latter one $PhCO_2^-$ group is chelating). On the basis of the wealth of uses and higher-nuclearity products obtained from reactions of the $[Mn_4O_2(O_2CPh)_9(H_2O)]^-$ ion,[10] complex **3** may also prove a good starting point for further synthetic chemistry.

Compound **4**·5CH_2Cl_2 crystallises in monoclinic space group $P2_1/a$. There is a $[Fe_4(\mu_3\text{-}O)_2]^{8+}$ core but it has an unusual asymmetry not previously observed in $[M_4(\mu_3\text{-}O)_2]$ species. All previous examples have had either the 'bent' (butterfly) or 'planar' dispositions of four metal ions, Types I and II, respectively, as

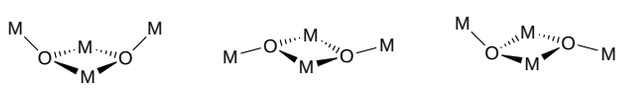

shown, with the pyramidal μ_3-O^{2-} ions either on the same side (Type I) or on opposite sides (Type II) of the fused Mn_3 planes. In contrast, **4** has a Type III core that is a hybrid of Types I and II. Thus, O(7) is 0.455 Å below the Fe(1)–Fe(2)–Fe(3) plane whereas O(8) is 0.206 Å *above* the Fe(1)–Fe(3)–Fe(4) plane. This is also reflected in the sum of angles at O(7) and O(8), which are 342.4 and 356.3°, respectively. It is interesting that O(7) is more pyramidal than the μ_3-O^{2-} in **3** whereas O(8) is less pyramidal; as a result, the dihedral angle between the two Mn_3 planes in **4** (143.63°) is only slightly larger than in **3** (142.15°). The asymmetric Type III structure has not been seen previously, although there is something similar in higher-nuclearity species such as $[Mn_7O_4(O_2CMe)_{10}(dbm)_4]^-$ [24] and $[Mn_8O_4(O_2CPh)_{12}(Et_2mal)_2(H_2O)_2]^{2-}$ (Et_2mal = 2,2-diethylmalonate).[10]

Compound **5** crystallises in triclinic space group $P\bar{1}$. The anion contains a Type I $[Fe_4(\mu_3\text{-}O)_2]^{8+}$ core very similar to that in the bpy complex **1**. The anion is also very similar to $[M_4O_2(O_2CMe)_7(pic)_2]^-$ (M = Mn [8] or Cr [15]) reported earlier. The μ_3-O^{2-} ions O(5) and O(6) are 0.318 and 0.299 Å, respectively, above their Fe_3 planes, with sum of angles of 351.15 and 352.11°, respectively; again, the degree of pyramidality of these oxygens in **5** is intermediate to the two types in Type III complex **4**.

It is interesting that both complexes **3** and **4** have two terminal Cl^- ligands but in **3** they are symmetrically disposed, one on each of the two wingtip metal atoms, whereas in **4** one is on a wingtip atom and one on a body atom. Also, the previously reported complex $[Fe_4O_2Cl_2(O_2CMe)_6(NC_5H_4Me\text{-}3)_4]$[5] has the same struc-

Table 2 Selected interatomic distances (Å) and angles (°) for $[Mn_4O_2Cl_2(O_2CC_6H_3F_2)_6(py)_4]$ **3**

Mn(1)···Mn(2)	3.418(2)	Mn(2)–O(66)	2.157(5)	Mn(1)–O(44)	2.184(5)	Mn(4)–Cl(8)	2.287(3)
Mn(2)···Mn(3)	2.875(2)	Mn(2)–N(15)	2.265(6)	Mn(1)–O(88)	1.985(5)	Mn(4)–O(6)	1.882(5)
Mn(2)···Mn(4)	3.314(2)	Mn(3)–O(5)	1.864(5)	Mn(1)–N(9)	2.075(6)	Mn(4)–O(57)	2.151(5)
Mn(1)···Mn(3)	3.294(2)	Mn(3)–O(6)	1.913(5)	Mn(2)–O(5)	1.922(5)	Mn(4)–O(68)	1.973(5)
Mn(3)···Mn(4)	3.361(2)	Mn(3)–O(46)	1.992(5)	Mn(2)–O(6)	1.876(5)	Mn(4)–O(79)	2.179(5)
Mn(1)–Cl(7)	2.296(2)	Mn(3)–O(77)	1.940(5)	Mn(2)–O(35)	1.933(5)	Mn(4)–N(27)	2.061(6)
Mn(1)–O(5)	1.874(5)	Mn(3)–O(90)	2.137(5)	Mn(2)–O(55)	2.010(5)		
Mn(1)–O(33)	2.149(5)	Mn(3)–N(21)	2.272(6)				
Cl(7)–Mn(1)–O(5)	90.0(2)	Cl(7)–Mn(1)–N(9)	89.9(2)	O(6)–Mn(2)–O(55)	97.8(2)	O(90)–Mn(3)–N(21)	165.1(2)
Cl(7)–Mn(1)–O(33)	95.10(14)	O(5)–Mn(1)–O(33)	93.1(2)	O(6)–Mn(2)–O(66)	90.8(2)	Cl(8)–Mn(4)–O(6)	90.6(2)
Cl(7)–Mn(1)–O(44)	91.97(14)	O(5)–Mn(1)–O(44)	98.4(2)	O(6)–Mn(2)–N(15)	97.3(2)	Cl(8)–Mn(4)–O(57)	91.94(14)
Cl(7)–Mn(1)–O(88)	175.2(2)	O(5)–Mn(1)–O(88)	94.7(2)	O(35)–Mn(2)–O(55)	85.8(2)	Cl(8)–Mn(4)–O(68)	174.5(2)
O(5)–Mn(1)–N(9)	177.2(2)	O(5)–Mn(3)–O(46)	97.9(2)	O(35)–Mn(2)–O(66)	83.8(2)	Cl(8)–Mn(4)–O(79)	93.26(14)
O(33)–Mn(1)–O(44)	166.5(2)	O(5)–Mn(3)–O(77)	176.0(2)	O(35)–Mn(2)–N(15)	88.8(2)	Cl(8)–Mn(4)–N(27)	91.1(2)
O(33)–Mn(1)–O(88)	85.8(2)	O(5)–Mn(3)–O(90)	90.4(2)	O(55)–Mn(2)–O(66)	85.3(2)	O(6)–Mn(4)–O(57)	95.2(2)
O(33)–Mn(1)–N(9)	84.1(2)	O(5)–Mn(3)–N(21)	95.1(2)	O(55)–Mn(2)–N(15)	82.1(2)	O(6)–Mn(4)–O(68)	94.9(2)
O(44)–Mn(1)–O(88)	86.2(2)	O(6)–Mn(3)–O(46)	174.2(2)	O(66)–Mn(2)–N(15)	165.8(2)	O(6)–Mn(4)–O(79)	95.5(2)
O(44)–Mn(1)–N(9)	84.5(2)	O(6)–Mn(3)–O(77)	95.5(2)	O(5)–Mn(3)–O(6)	81.4(2)	O(6)–Mn(4)–N(27)	178.3(2)
O(88)–Mn(1)–N(9)	85.5(2)	O(6)–Mn(3)–O(90)	100.3(2)	O(57)–Mn(4)–O(68)	87.0(2)	Mn(1)–O(5)–Mn(2)	128.4(3)
O(5)–Mn(2)–O(6)	80.9(2)	O(6)–Mn(3)–N(21)	94.2(2)	O(57)–Mn(4)–O(79)	168.1(2)	Mn(1)–O(5)–Mn(3)	123.6(3)
O(5)–Mn(2)–O(35)	96.0(2)	O(46)–Mn(3)–O(77)	85.4(2)	O(57)–Mn(4)–N(27)	84.7(2)	Mn(2)–O(5)–Mn(3)	98.8(2)
O(5)–Mn(2)–O(55)	175.4(2)	O(46)–Mn(3)–O(90)	85.5(2)	O(68)–Mn(4)–O(79)	86.8(2)	Mn(2)–O(6)–Mn(3)	98.7(2)
O(5)–Mn(2)–O(66)	99.1(2)	O(46)–Mn(3)–N(21)	80.1(2)	O(68)–Mn(4)–N(27)	83.5(2)	Mn(2)–O(6)–Mn(4)	123.7(2)
O(5)–Mn(2)–N(15)	93.7(2)	O(77)–Mn(3)–O(90)	87.6(2)	O(79)–Mn(4)–N(27)	84.5(2)	Mn(3)–O(6)–Mn(4)	124.7(3)
O(6)–Mn(2)–O(35)	173.3(2)	O(77)–Mn(3)–N(21)	87.6(2)				

Table 3 Selected interatomic distances (Å) and angles (°) for $[Fe_4O_2Cl_2(O_2CMe)_6(bpy)_2]$ **4**

Fe(1)···Fe(3)	2.896(5)	Fe(2)–N(33)	2.18(2)	Fe(1)–O(9)	2.050(4)	Fe(4)–Cl(5)	2.331(6)
Fe(1)···Fe(2)	3.421(6)	Fe(2)–N(44)	2.14(2)	Fe(1)–O(21)	2.010(4)	Fe(4)–O(8)	1.822(12)
Fe(1)···Fe(4)	3.487(6)	Fe(3)–O(7)	1.938(12)	Fe(1)–O(31)	2.041(4)	Fe(4)–O(27)	2.037(4)
Fe(2)···Fe(3)	3.234(5)	Fe(3)–O(8)	1.931(12)	Fe(2)–O(7)	1.807(12)	Fe(4)–O(29)	1.999(4)
Fe(3)···Fe(4)	3.394(5)	Fe(3)–O(15)	2.027(3)	Fe(2)–O(11)	2.020(4)	Fe(4)–N(45)	2.20(2)
Fe(1)–Cl(6)	2.376(8)	Fe(3)–O(19)	2.047(4)	Fe(2)–O(13)	2.037(3)	Fe(4)–N(56)	2.17(2)
Fe(1)–O(7)	1.990(12)	Fe(3)–O(23)	2.025(4)	Fe(2)–O(17)	2.012(4)		
Fe(1)–O(8)	1.994(13)	Fe(3)–O(25)	2.008(4)				
Cl(6)–Fe(1)–O(7)	95.8(4)	O(7)–Fe(1)–O(8)	81.0(5)	O(11)–Fe(2)–N(33)	81.7(5)	Cl(5)–Fe(4)–O(8)	100.3(4)
Cl(6)–Fe(1)–O(8)	174.8(4)	O(7)–Fe(1)–O(9)	91.4(4)	O(11)–Fe(2)–N(44)	92.1(5)	Cl(5)–Fe(4)–O(27)	92.7(2)
Cl(6)–Fe(1)–O(9)	89.2(2)	O(7)–Fe(1)–O(21)	92.7(4)	O(13)–Fe(2)–O(17)	88.5(2)	Cl(5)–Fe(4)–O(29)	94.6(2)
Cl(6)–Fe(1)–O(21)	86.8(2)	O(7)–Fe(1)–O(31)	173.6(4)	O(13)–Fe(2)–N(33)	85.2(5)	Cl(5)–Fe(4)–N(45)	92.8(5)
Cl(6)–Fe(1)–O(31)	90.5(2)	O(8)–Fe(1)–O(9)	95.0(4)	O(13)–Fe(2)–N(44)	88.0(5)	Cl(5)–Fe(4)–N(56)	166.2(4)
O(8)–Fe(1)–O(21)	89.3(4)	O(7)–Fe(3)–O(23)	90.6(4)	O(17)–Fe(2)–N(33)	86.7(5)	O(8)–Fe(4)–O(27)	96.5(4)
O(8)–Fe(1)–O(31)	92.8(3)	O(7)–Fe(3)–O(25)	175.4(4)	O(17)–Fe(2)–N(44)	161.0(4)	O(8)–Fe(4)–O(29)	98.2(4)
O(9)–Fe(1)–O(21)	1745.5(2)	O(8)–Fe(3)–O(15)	175.6(4)	N(33)–Fe(2)–N(44)	74.3(6)	O(8)–Fe(4)–N(45)	166.4(6)
O(9)–Fe(1)–O(31)	87.7(2)	O(8)–Fe(3)–O(19)	92.5(4)	O(7)–Fe(3)–O(8)	83.9(5)	O(8)–Fe(4)–N(56)	93.5(6)
O(21)–Fe(1)–O(31)	88.6(2)	O(8)–Fe(3)–O(23)	92.2(4)	O(7)–Fe(3)–O(15)	91.7(4)	O(27)–Fe(4)–O(29)	162.1(2)
O(7)–Fe(2)–O(11)	98.5(4)	O(8)–Fe(3)–O(25)	97.8(4)	O(7)–Fe(3)–O(19)	97.4(4)	O(27)–Fe(4)–N(45)	78.9(5)
O(7)–Fe(2)–O(13)	95.1(4)	O(15)–Fe(3)–O(19)	88.7(2)	O(27)–Fe(4)–N(56)	87.0(5)	Fe(1)–O(7)–Fe(3)	95.0(5)
O(7)–Fe(2)–O(17)	103.0(4)	O(15)–Fe(3)–O(23)	87.1(2)	O(29)–Fe(4)–N(45)	84.5(5)	Fe(2)–O(7)–Fe(3)	119.3(7)
O(7)–Fe(2)–N(33)	170.2(7)	O(15)–Fe(3)–O(25)	86.52(13)	O(29)–Fe(4)–N(56)	82.1(5)	Fe(1)–O(8)–Fe(3)	95.1(5)
O(7)–Fe(2)–N(44)	95.9(6)	O(19)–Fe(3)–O(23)	171.1(2)	N(45)–Fe(4)–N(56)	73.6(6)	Fe(1)–O(8)–Fe(4)	132.0(7)
O(11)–Fe(2)–O(13)	166.2(2)	O(19)–Fe(3)–O(25)	86.8(2)	Fe(1)–O(7)–Fe(2)	128.1(7)	Fe(3)–O(8)–Fe(4)	129.2(7)
O(11)–Fe(2)–O(17)	87.0(2)	O(23)–Fe(3)–O(25)	85.04(12)				

ture as that of the Mn_4 complex **3** so that two different arrangements of two Cl^- ions on the $[Fe_4O_2]$ core have now been seen.

Magnetic susceptibility studies

Variable-temperature, solid-state, magnetic susceptibility (χ_m) studies have been performed on powdered samples of complex **4** in the temperature range 12.0 to 294 K. Complexes **3** and **5** were not studied since such Type I butterfly complexes for both Mn^{III} and Fe^{III} have been reported on multiple occasions previously.[3,4,7,8]

The effective magnetic moment (μ_{eff}) per Fe_4 slowly decreases from 4.59 μ_B at 294 K to 0.80 μ_B at 14.0 K and then slightly increases to 0.82 μ_B at 12.0 K (Fig. 4). These correspond to $\chi_m T$ values of 2.63, 0.080 and 0.084 cm^3 K mol^{-1}, respectively. The data are suggestive of an antiferromagnetically coupled system with an $S = 0$ ground state, the small 'tail' at low T being the signature of paramagnetic impurities. For a complex such as **4** with C_1 symmetry a total of five exchange parameters J_{ij} are required for each possible pairwise exchange interaction between iron(III) atoms i and j; a sixth parameter J_{24} is assumed to be zero, given the large distance involved. However, the main exchange interaction pathway will be *via* the μ_3-O^{2-} bridges, not the acetate bridges, so that, from a magnetism viewpoint, the core symmetry is C_s and only three J values are required: $J_{14} = J_{34} = J_{wb}$; $J_{12} = J_{23} = J_{wb}'$; and $J_{13} = J_{bb}$, where b = body and w = wingtip. In fact, consideration of the Fe–O and Fe–O–Fe distances and angles in Table 3 shows that the slight difference in pyramidality between O(7) and O(8) has little influence on these structural parameters, and a 2J model appropriate for C_{2v} symmetry, *i.e.* $J_{wb} = J_{wb}'$, thus does not appear unreasonable. This model is also the one employed previously for **1** and discussed in detail elsewhere.[3] The derived μ_{eff} *vs.* T expression for a $2J(C_{2v})$ model gave a good fit, shown as a solid line in Fig. 4, supporting the reasonableness of the 2J model. The fitting parameters were $J_{wb} = -4.1$ cm^{-1}, $J_{bb} = -10.9$ cm^{-1}, $g = 1.93$

Table 4 Selected interatomic distances (Å) and angles (°) for $[NBu^n_4][Fe_4O_2(O_2CMe)_7(pic)_2]$ **5**

Fe(1)···Fe(3)	2.843(2)	Fe(2)–O(41)	2.125(5)	Fe(1)–O(29)	2.070(5)	Fe(4)–O(6)	1.844(5)
Fe(1)···Fe(2)	3.463(2)	Fe(2)–N(7)	2.153(6)	Fe(1)–O(47)	2.069(5)	Fe(4)–O(23)	2.030(5)
Fe(1)···Fe(4)	3.315(2)	Fe(3)–O(5)	1.912(5)	Fe(1)–O(51)	2.018(5)	Fe(4)–O(35)	2.086(5)
Fe(2)···Fe(3)	3.332(2)	Fe(3)–O(6)	1.941(5)	Fe(2)–O(5)	1.844(5)	Fe(4)–O(45)	1.999(5)
Fe(3)···Fe(4)	3.476(2)	Fe(3)–O(31)	2.043(5)	Fe(2)–O(14)	2.020(5)	Fe(4)–O(49)	2.056(5)
Fe(1)–O(5)	1.954(5)	Fe(3)–O(33)	2.010(5)	Fe(2)–O(27)	2.052(5)	Fe(4)–N(16)	2.166(6)
Fe(1)–O(6)	1.915(5)	Fe(3)–O(39)	2.108(5)	Fe(2)–O(37)	1.998(5)		
Fe(1)–O(25)	2.011(5)	Fe(3)–O(43)	2.027(5)				
O(5)–Fe(1)–O(6)	84.2(2)	O(5)–Fe(1)–O(51)	173.4(2)	O(14)–Fe(2)–O(37)	91.6(2)	O(39)–Fe(3)–O(43)	90.3(2)
O(5)–Fe(1)–O(25)	90.7(2)	O(6)–Fe(1)–O(25)	174.3(2)	O(14)–Fe(2)–O(41)	86.0(2)	O(6)–Fe(4)–O(23)	169.9(2)
O(5)–Fe(1)–O(29)	87.1(2)	O(6)–Fe(1)–O(29)	89.1(2)	O(14)–Fe(2)–N(7)	77.2(2)	O(6)–Fe(4)–O(35)	92.5(2)
O(5)–Fe(1)–O(47)	96.5(2)	O(6)–Fe(1)–O(47)	89.6(2)	O(27)–Fe(2)–O(37)	101.5(2)	O(6)–Fe(4)–O(45)	94.6(2)
O(6)–Fe(1)–O(51)	96.0(2)	O(5)–Fe(3)–O(31)	91.2(2)	O(27)–Fe(2)–O(41)	167.6(2)	O(6)–Fe(4)–O(49)	96.5(2)
O(25)–Fe(1)–O(29)	93.2(2)	O(5)–Fe(3)–O(33)	169.1(2)	O(27)–Fe(2)–N(7)	85.3(2)	O(6)–Fe(4)–N(16)	93.9(2)
O(25)–Fe(1)–O(47)	88.5(2)	O(5)–Fe(3)–O(39)	88.7(2)	O(37)–Fe(2)–O(41)	88.8(2)	O(23)–Fe(4)–O(35)	82.8(2)
O(25)–Fe(1)–Fe(51)	89.31(2)	O(5)–Fe(3)–O(43)	96.0(2)	O(37)–Fe(2)–N(7)	166.7(2)	O(23)–Fe(4)–O(45)	94.5(2)
O(29)–Fe(1)–O(47)	176.1(2)	O(6)–Fe(3)–O(31)	86.5(2)	O(41)–Fe(2)–N(7)	83.3(2)	O(23)–Fe(4)–O(49)	87.7(2)
O(29)–Fe(1)–O(51)	86.3(2)	O(6)–Fe(3)–O(33)	90.1(2)	O(5)–Fe(3)–O(6)	84.7(2)	O(23)–Fe(4)–N(16)	77.2(2)
O(47)–Fe(1)–O(51)	90.2(2)	O(6)–Fe(3)–O(39)	98.1(2)	O(35)–Fe(4)–O(45)	92.2(2)	Fe(1)–O(5)–Fe(2)	131.5(3)
O(5)–Fe(2)–O(14)	171.1(2)	O(6)–Fe(3)–O(43)	171.6(2)	O(35)–Fe(4)–O(49)	170.2(2)	Fe(1)–O(5)–Fe(3)	94.7(2)
O(5)–Fe(2)–O(27)	92.1(2)	O(31)–Fe(3)–O(33)	98.1(2)	O(35)–Fe(4)–N(16)	90.0(2)	Fe(2)–O(5)–Fe(3)	125.0(3)
O(5)–Fe(2)–O(37)	97.3(2)	O(31)–Fe(3)–O(39)	175.4(2)	O(45)–Fe(4)–O(49)	90.7(2)	Fe(1)–O(6)–Fe(3)	95.0(2)
O(5)–Fe(2)–O(41)	93.6(2)	O(31)–Fe(3)–O(43)	85.14(2)	O(45)–Fe(4)–N(16)	171.0(2)	Fe(1)–O(6)–Fe(4)	123.7(3)
O(5)–Fe(2)–N(7)	93.9(2)	O(33)–Fe(3)–O(39)	82.6(2)	O(49)–Fe(4)–N(16)	85.7(2)	Fe(3)–O(6)–Fe(4)	133.4(3)
O(14)–Fe(2)–O(27)	86.7(2)	O(33)–Fe(3)–O(43)	99.6(2)				

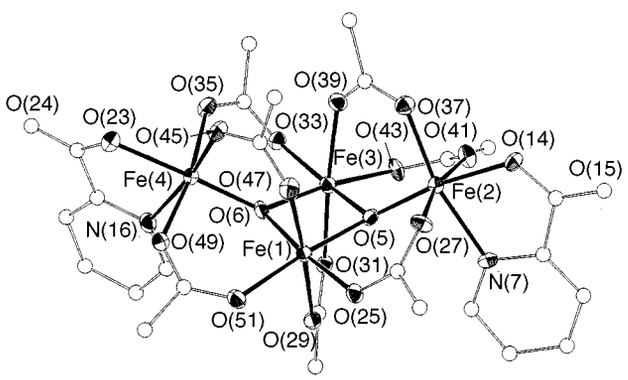

Fig. 3 An ORTEP representation of the anion of complex **5**. Details as in Fig. 2

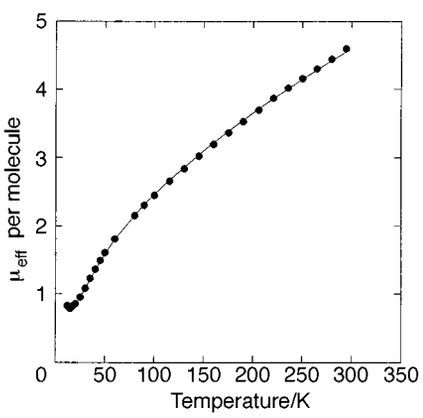

Fig. 4 Plot of effective magnetic moment (μ_{eff}) per Fe_4 molecule *vs.* temperature for $[Fe_4O_2Cl_2(O_2CMe)_6(bpy)_2]$ **4**. The solid line is a fit of the experimental data to the 2*J* model; see the text for the fitting parameters

and PAR = 0.016, where the latter is the mole ratio of paramagnetic impurity (assumed to be mononuclear Fe^{III}). Temperature-independent magnetism was held constant at 800×10^{-6} cm^3 mol^{-1}. The obtained *J* values compare closely with those previously determined for **1**: $J_{bb} = -8.9$ cm^{-1}, $J_{wb} = -45.5$ cm^{-1} and $g = 2.0$.[3] As for **1**, the ground state of **4** is $S = 0$. Also as for **1**, an error-surface plot for the fitting shows that while the value of J_{wb} is well determined by the fitting procedure, the value of J_{bb} is not: since J_{wb} is so much stronger than J_{bb}, and since there are four J_{wb} interactions and only one J_{bb}, the spin-manifold energies are primarily determined by J_{wb}, making the precise value of J_{bb} indeterminate. Thus, as for **1**, a large range of J_{bb} values give essentially equally good fits of the data, although the quoted J_{bb} does give the lowest fitting error.

The main conclusion to be drawn from the magnetic studies is that the structural differences between the Type III complex **4** and **1** do not cause significant changes to the magnetic properties of the $[Fe_4O_2]^{8+}$ core.

Mössbauer spectroscopy

The ^{57}Fe Mössbauer spectra of complex **4** were recorded at 120 and 210 K and are shown in Fig. 5. The broad doublet observed at each temperature can be fit by two doublets of equal area whose isomer shifts (δ) and quadrupole splitting (ΔE_Q) values are listed in Table 5. Within the resolution of the Mössbauer experiment, there are thus only two inequivalent types of Fe in **4**, contrasting with its C_1 symmetry but nevertheless consistent with the arguments above that the differences between the two body atoms and between the two wingtip atoms are not very large on an absolute scale. Thus, the two doublets are assigned to the body and wingtip pairs of iron(III) atoms. The two δ values at each temperature are similar, are consistent with high-spin Fe^{III}, and show little temperature dependence. They are similar to those obtained previously for **1** [0.459(2) and 0.495(3) mm s^{-1} at 200 K, and 0.457(2) and 0.487(2) mm s^{-1} at 105 K],[3] consistent with the similar iron(III) environments in the two molecules. The ΔE_Q values for both sites in **4** reflect deviations from octahedral geometry, since the valence-electron contribution to ΔE_Q is negligible for a high-spin iron(III) ion. The two ΔE_Q are also significantly different by almost a factor of two. The larger ΔE_Q of ≈1.1 mm s^{-1} is assigned to the wingtip iron atoms Fe(2) and Fe(4) that show the greater variety of ligand-atom type and larger bond length range of 1.807(12)–2.201(17) Å, excluding Fe(1)–Cl(6) [2.376(8) Å]. In contrast, the body iron atoms have only an O-based environment and, more importantly, a bond length range of only 1.931(12)–2.050(4) Å, excluding Fe(1)–Cl(6) [2.376(8) Å]. The larger bond length range for wingtip atoms is caused by the short Fe(2)–O(7) and Fe(4)–O(8) bonds and their *trans* influence on Fe(2)–N(33) and Fe(4)–N(45). The short Fe–O^{2-} bonds for the wingtip atoms provide the primary distortion of the co-ordination geometry from octahedral and are thus the primary contributors to the

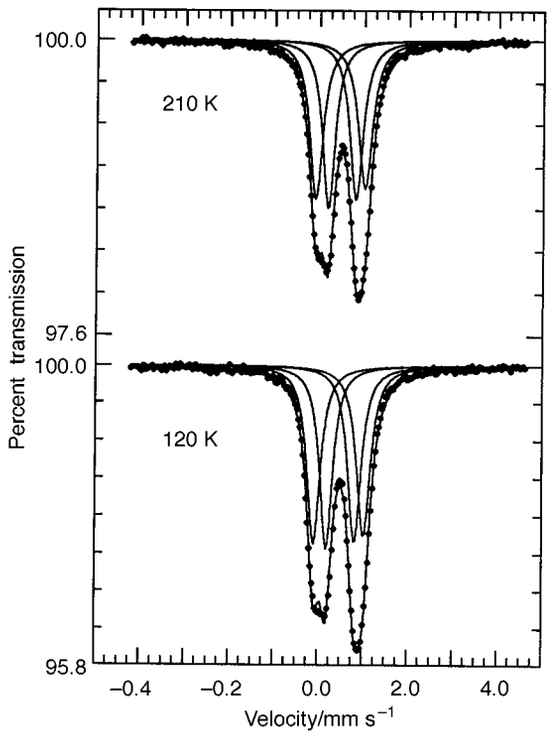

Fig. 5 The ^{57}Fe Mössbauer spectra for $[Fe_4O_2Cl_2(O_2CMe)_6(bpy)_2]$ **4** at 120 and 210 K. The solid line is a fit of the data with the two equal-area doublets shown. See Table 5 for the fitting parameters

Table 5 Mössbauer parameters for $[Fe_4O_2Cl_2(O_2CMe)_6(bpy)_2]$ **4**

T/K	δ[a]/mm s^{-1}	ΔE_Q/mm s^{-1}	Γ[b]/mm s^{-1}	−ln(area)[c]
210	0.472(2)	1.101(3)	0.181(2), 0.171(2)	−0.160(4)
	0.513(2)	0.619(3)	0.180(3), 0.194(3)	
120	0.471(2)	1.115(3)	0.179(3), 0.174(2)	+0.484(4)
	0.511(2)	0.631(3)	0.181(3), 0.187(3)	

[a] Isomer shift relative to iron foil at room temperature. [b] Full width at half height; the width for the line at more negative velocity is listed first for each doublet. [c] Minus the natural logarithm of the background-normalized spectral area.

greater ΔE_Q value. Similar ΔE_Q differences were observed between wingtip and body iron atoms in **1** [1.305(5)/0.960(6) mm s^{-1} at 200 K and 1.333(3)/0.962(4) mm s^{-1} at 105 K] where Fe^{III}–O^{2-} bonds for wingtip atoms [1.819(5) Å] were again much shorter than for body atoms [1.926(5), 1.947(5) Å].[3] In contrast, in $[NEt_4][Fe_4O_2(O_2CPh)_7\{H_2B(pz)_2\}_2]$,[2] the differences in Fe^{III}–O^{2-} bond lengths between body and wingtip atoms are not as great and the complex exhibits a single quadrupole doublet with, *e.g.*, $\delta = 0.45$ mm s^{-1} and $\Delta E_Q = 1.20$ mm s^{-1} at 230 K. Thus, in this complex, the iron(III) atoms are all equivalent as far as the Mössbauer technique is concerned.

Conclusion

The present work has provided convenient access to two new $[M_4O_2]$ species that contain Cl^- terminal ligands. These could have future utility as sites for facile incorporation of other ligands by metathesis or as means to access higher-nuclearity species; the latter possibility is supported by several results over the last few years showing how $[NBu^n_4][Mn_4O_2(O_2CPh)_9(H_2O)]$ has proven an excellent starting point for new clusters with metal nuclearities up to 18.[27] The iron complex $[Fe_4O_2Cl_2(O_2CMe)_6(bpy)_2]$ **4** has an asymmetric core not previously seen in a discrete, tetranuclear complex, but combined magnetochemical and Mössbauer data indicate that this asymmetry does not markedly affect the observed properties of the core. The complex $[NBu^n_4][Fe_4O_2(O_2CMe)_7(pic)_2]$ **5** and its $PhCO_2^-$ analogue **6** provide new examples of Fe_4O_2 species and join the previously prepared Mn^{III}_4 and Cr^{III}_4 analogues.

Acknowledgements

This work was supported by the US National Science Foundation.

References

1 V. I. Ponomarev, L. O. Atovmyan, S. A. Bobkova and K. I. Turté, *Dokl. Akad. Nauk. SSSR*, 1984, **274**, 368.
2 W. H. Armstrong, M. E. Roth and S. J. Lippard, *J. Am. Chem. Soc.*, 1987, **109**, 6318.
3 J. K. McCusker, J. B. Vincent, E. A. Schmitt, M. L. Mino, K. Shin, D. K. Coggin, P. M. Hagen, J. C. Huffman, G. Christou and D. N. Hendrickson, *J. Am. Chem. Soc.*, 1991, **113**, 3012.
4 P. Chaudhuri, M. Winter, P. Fleischhauer, W. Haase, U. Florke and H.-J. Haupt, *Inorg. Chim. Acta*, 1993, **212**, 241.
5 L. Wu, M. Pressprich, P. Coppens and M. J. DeMarco, *Acta Crystallogr., Sect. C*, 1993, **49**, 1255.
6 S. M. Gorun and S. J. Lippard, *Inorg. Chem.*, 1988, **27**, 149.
7 (*a*) J. B. Vincent, C. Christmas, J. C. Huffman, G. Christou, H.-R. Chang and D. N. Hendrickson, *J. Chem. Soc., Chem. Commun.*, 1987, 236; (*b*) J. B. Vincent, C. Christmas, H.-R. Chang, Q. Li, P. D. W. Boyd, J. C. Huffman, D. N. Hendrickson and G. Christou, *J. Am. Chem. Soc.*, 1989, **111**, 2086.
8 E. Libby, J. K. McCusker, E. A. Schmitt, K. Folting, D. N. Hendrickson and G. Christou, *Inorg. Chem.*, 1991, **30**, 3486.
9 E. Bouwman, M. A. Bolcar, E. Libby, J. C. Huffman, K. Folting and G. Christou, *Inorg. Chem.*, 1992, **31**, 5185.
10 M. W. Wemple, H.-L. Tsai, S. Wang, J.-P. Claude, W. E. Streib, J. C. Huffman, D. N. Hendrickson and G. Christou, *Inorg. Chem.*, 1996, **35**, 6437.
11 S. K. Chandra, P. Chakraborty and A. Chakravorty, *J. Chem. Soc., Dalton Trans.*, 1993, 863.
12 M. Mikuriya, Y. Yamato and T. Tokii, *Chem. Lett.*, 1991, 1429.
13 C. Gedye, C. Harding, V. McKee, J. Nelson and J. Patterson, *J. Chem. Soc., Chem. Commun.*, 1992, 392.
14 H. H. Thorp, J. E. Sarneski, R. J. Kulawiec, G. W. Brudvig, R. H. Crabtree and G. C. Papaefthymiou, *Inorg. Chem.*, 1991, **30**, 1153.
15 (*a*) A. Bino, R. Chayat, E. Pedersen and A. Schneider, *Inorg. Chem.*, 1991, **30**, 856; (*b*) T. Ellis, M. Glass, A. Harton, K. Folting, J. C. Huffman and J. B. Vincent, *Inorg. Chem.*, 1994, **33**, 5522.
16 S. L. Castro, Z. Sun, J. C. Bollinger, D. N. Hendrickson and G. Christou, *J. Chem. Soc., Chem. Commun.*, 1995, 2517.
17 D. N. Hendrickson, G. Christou, E. A. Schmitt, E. Libby, J. S. Bashkin, S. Wang, H.-L. Tsai, J. B. Vincent, P. D. W. Boyd, J. C. Huffman, K. Folting, Q. Li and W. E. Streib, *J. Am. Chem. Soc.*, 1992, **114**, 2455.
18 J. B. Vincent, J. C. Huffman, G. Christou, Q. Li, M. A. Nanny, D. N. Hendrickson, R. H. Fong and R. H. Fish, *J. Am. Chem. Soc.*, 1988, **110**, 6898.
19 M. W. Wemple, H.-L. Tsai, K. Folting, D. N. Hendrickson and G. Christou, *Inorg. Chem.*, 1993, **32**, 2025.
20 (*a*) M. H. Chisholm, K. Folting, J. C. Huffman and C. C. Kirkpatrick, *Inorg. Chem.*, 1984, **23**, 1021; (*b*) A. C. Larson, The LASL Crystal Structure Program Library, Los Alamos Laboratory of the University of California, Los Alamos, New Mexico, 1971.
21 P. Main, S. J. Fiske, S. E. Hill, L. Lessinger, G. Germain, J.-P. Declerq and M. M. Woolfson, MULTAN 78, University of York and Louvain, 1978.
22 M. J. Cohn, M. D. Timken and D. N. Hendrickson, *J. Am. Chem. Soc.*, 1984, **106**, 6683.
23 B. L. Chrisman and T. A. Tumolillo, *Comput. Phys. Commun.*, 1971, **2**, 322.
24 S. Wang, H.-L. Tsai, W. E. Streib, G. Christou and D. N. Hendrickson, *J. Chem. Soc., Chem. Commun.*, 1992, 677.
25 A. R. Schake, J. B. Vincent, Q. Li, P. D. W. Boyd, K. Folting, J. C. Huffman, D. N. Hendrickson and G. Christou, *Inorg. Chem.*, 1989, **28**, 1915.
26 J. B. Vincent, H.-L. Tsai, A. G. Blackman, S. Wang, P. D. W. Boyd, K. Folting, J. C. Huffman, E. B. Lobkovsky, D. N. Hendrickson and G. Christou, *J. Am. Chem. Soc.*, 1993, **115**, 12 353.
27 R. C. Squire, S. M. J. Aubin, K. Folting, W. E. Streib, G. Christou and D. N. Hendrickson, *Inorg. Chem.*, 1995, **34**, 6463.

Received 15*th September* 1997; *Paper* 7/06668F